processes

MDPI

Article

Cause Analysis of Condensed Water Induced Bulging in High-Pressure Steam Tee Joints of a Pyrolyzer

Weiqi Lian [1,2], Zhiwei Sun [1], Yunrong Lyu [1,*] and Zhihong Duan [1,*]

[1] Guangdong Provincial Key Laboratory of Petrochemical Equipment Fault Diagnosis, Guangdong University of Petrochemical Technology, Maoming 525000, China; lianwq@gdupt.edu.cn (W.L.); 18218895416@163.com (Z.S.)
[2] College of Mechanical and Electrical Engineering, Guangdong University of Petrochemical Technology, Maoming 525000, China
* Correspondence: lyclyr@yeah.net (Y.L.); 13727781119@163.com (Z.D.)

Abstract: High-pressure steam pipes inevitably suffered from the reciprocal interaction of high pressure and temperature during a long-period service, causing deformation and cracking. However, only limited studies about abnormal bulging caused by condensed water have been carried out. To study the relationship between bulging and condensed water, bulging tee joints belonging to high-pressure steam pipes were investigated with a macro visual inspection, chemical composition analysis, and metallographic microscopy. According to the analysis of the bulging samples, pearlite spheroidization was found in the abnormal bulging tee joint. The ANSYS FLUENT modeling indicated that the tube wall of bulging tees was continuously subjected to alternating stress, causing the cyclic transformation of the liquid–gas phase inside the tee joint. The results indicate that the stress produced by a condensed water droplet ranges from 532.8 MPa to 59 MPa, continuously exerting pressure on the tube wall of the tee joint. When combined with the variation in the temperature field, the temperature of the severe bulging tee joint and slight bulging tee joint alternates. Further modeling illustrates that the stress generated by the impact of condensed water droplets on the high-temperature tee joints causes a ratcheting effect, which is identified as the main factor contributing to the bulging of the tee joint. Deterioration of the microstructure is considered a secondary mechanism.

Keywords: bulging; tee joint; condensed water; ratcheting; altering thermal stress

Citation: Lian, W.; Sun, Z.; Lyu, Y.; Duan, Z. Cause Analysis of Condensed Water Induced Bulging in High-Pressure Steam Tee Joints of a Pyrolyzer. *Processes* **2023**, *11*, 2288. https://doi.org/10.3390/pr11082288

Academic Editor: Kian Jon Chua

Received: 24 June 2023
Revised: 20 July 2023
Accepted: 28 July 2023
Published: 30 July 2023

1. Introduction

High-pressure steam pipes, one of the most critical pieces of equipment connecting the boiler system and turbo generator, are prone to deform and cracking during a long period of service when subjected to the reciprocal interaction of high pressure and temperature [1–3]. Pipe failure accidents in thermal power plants severely influence the long-period safety of operations. During the routine operation period, the internal temperature of high-pressure steam pipes could range from room temperature to nearly 540 °C, in which the pipe may be subjected to cyclic heating and forced cooling [4–7]. In many service conditions, damage occurs at local positions including pipe bends, welding lines and tee joints, etc., which results in pipe damage at these locations.

The tee junction, the main transport pipe fitting applied in a pipeline system, is widely used in the transportation of high-pressure gas and oil, which demands high reliability [8,9]. The failure rate of tee junctions due to erosion and perforation is increasingly annually. As the service condition and welding technique become more and more complicated, the thickness of tube walls for tee and pipes is uneven, increasing the failure risk due to the stress concentration effects [8,10,11]. A considerable amount of published work is available on the failure of tee joints near the welding line. Ashrafizadeh et al. conducted an analysis of a high-pressure natural gas pipe under split tee near a circular welding line via computer simulations and a metallurgical assessment; this research indicated that the presence of

large periodic stress was responsible for the initiation and fatigue propagation of the crack in the gas pipe [12]. Zheng et al. investigated a tee joint crack of a subcritical power station boiler final superheater header; they found that it belongs to a reheat crack and continuously propagates under excessive welding residual stress [13]. Cao et al. demonstrated a girth weld crack of a tee pipe, which originates from slag inclusion and propagates under the effect of stress concentration [14]. Kumar et al. presented a failure investigation of two different boiler tubes in a thermal power plant made of T22 grade. The results conclude that the first tube failed due to creep damage and another tube failed due to the combined effect of erosion and corrosion [15].

Based on the research mentioned above, previous studies have mainly focused on the influence of individual factors such as creep or residual stress on the failure of tee junctions. However, there have been limited investigations into the combined effects of diverse factors leading to the failure of high-temperature steam pipes. In actual working conditions, the medium inside the high-temperature steam pipe is a complex combination of steam and condensed water. Moreover, the medium within the high-temperature steam pipeline can experience a gas–liquid two-phase flow, resulting in alternating differential temperature stress acting on the pipe. Lyu et al. conducted a study on the failure mechanism of bulging and cracking in high-pressure steam pipes, employing physical and chemical inspections alongside numerical simulations. The results indicate that an excessive distance between the steam drain valve and the main steam pipe leads to constant condensation and the vaporization of condensed water within high-pressure steam pipes, resulting in alternating thermal stress and subsequent thermal fatigue [16]. In another study, Zhang et al. investigated the cause of cracks in the connection pipeline of a subcritical boiler reheater. They attributed the cracks to alternating thermal stress and non-periodic vibrations in the straight pipe and elbow arranged after fine-tuning the refrigerant flow direction in the reheater [17].

Due to long periods of operations at high temperatures, the microstructure of high-temperature steam pipes is susceptible to material deterioration, leading to the spheroidization and formation of creep voids. Munda et al. conducted a study on the mechanism of over-temperature failure in SA210 pipes, and they found that overheating conditions led to the degeneration of the initial ferrite–pearlite microstructure. Spheroidization and the coalescence of carbides occurred in the ferrite matrix of the boiler tube near the ruptured region, altering the initial ferrite–pearlite microstructure [18]. In a separate study, Rodrigo et al. observed partial cementite spheroidization in the heat-affected zone, which resulted in a significant decrease in hardness and tensile strength and correlated with localized dipping, rolling contact fatigue, and failures [19]. Furthermore, Khalifa et al. reported an early corrosion failure in the piping system of a gas heater. Some elbows in the system showed an early stage of carbide spheroidization and pearlite decomposition, which ultimately contributed to the final failure [20].

Therefore, the failure of high-pressure steam pipes is not solely influenced by residual stress but is also affected by various factors, including phase transitions of the internal medium and deterioration of the metallographic structure. However, there are only a few published studies available that are relevant to the failure of tee joints induced by condensed water, and the failure mechanism under diverse factors remains unclear. Therefore, it is essential to investigate the impact of these diverse factors on the failure of high-pressure steam pipes to ensure the safety and reliability of thermal power plant systems.

In this study, the authors conducted a failure analysis of a bulging tee joint located in a high-pressure steam pipe. Additionally, a systematic analysis was performed to determine the failure mechanism related to the presence of condensed water, which is generated under normal service conditions. The authors anticipate that this research will offer valuable insights to extend the service life of high-pressure steam pipes in petrochemical industries.

In October 2019, a pyrolyzer, belonging to a Chinese petrochemical enterprise, was shut down to overhaul. During the basic investigation, a high-pressure steam tee joint located between a ultra-high pressure main pipe and medium pressure pipe was found to

have abnormal bulging, while the external diameter increased from Φ219 mm to Φ243 mm. Meanwhile, the same phenomenon was discovered in another tee joint connecting the main pipe and safety valve branch pipe, whose external diameter increased from Φ219 mm to Φ226 mm. P11(1.25 Cr–0.5 Mo) alloy steel was selected as the design material for the high-pressure steam pipe. The operating pressure and temperature are 12 MPa and 500–540 °C, respectively.

The failure tee joints have been in service for 20 years since March 1999. After the overhaul, the abnormal bulging tee joints were investigated to find out the cause of the failure.

2. Experimental Failure Analysis

2.1. Visual Inspection and Sampling

The sampling location of the macro image for the abnormal bulging tee joint is shown in Figure 1a, including the slight bulging part (marked with A), straight pipe part (between A and B) and severe bulging part (marked with B). The branch pipes connected with the regulating valve and safety valve are marked with C and D, respectively. Furthermore, the detailed location of A, B, C and D are depicted in the schematic image of the abnormal bulging tee joint (Figure 1b). The specification of the tee joint is DN200, while the external diameter, internal diameter and thickness are 219 mm, 166.2 mm and 26.4 mm, respectively. According to the SCH160 standard, the relevant external diameter, internal diameter and thickness are 219 mm, 171 mm and 24 mm, respectively.

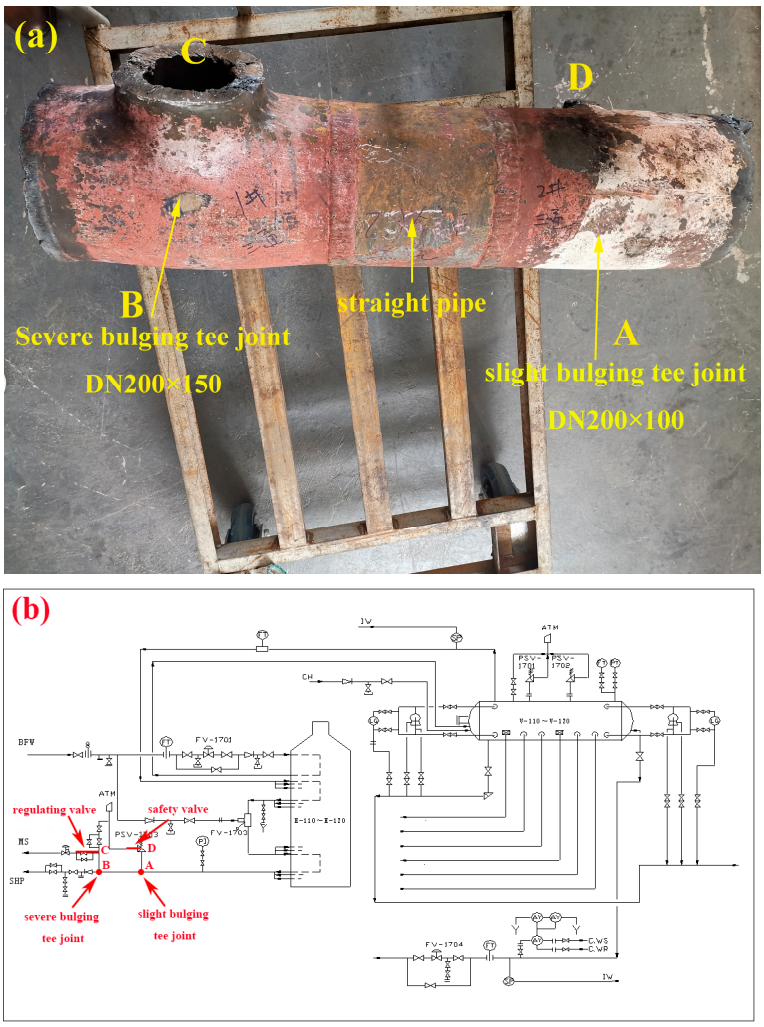

Figure 1. (**a**) Macro image of the bulging tee joint; (**b**) schematic location of the bulging and cracking pipe.

2.2. Thickness and External Diameter Measurement

Thickness measurements were conducted on all the sampled parts. The sampling location of the macro image for the abnormal bulging tee joint is shown in Figure 2a, including the slight bulging part (location 1–location 5), straight pipe part (location 6–location 8) and severe bulging part (location 9–location 12). The thickness data of each location were collected more than 10 times from different axial directions and then the results were averaged. As shown in Figure 2b,c, the thickness of all the sampled parts exceeds 24 mm. The slight bulging part exhibited a maximum thickness of 36.8 mm and a minimum thickness of 25.4 mm, while the straight parts had thicknesses ranging from 26.6 mm to 25.4 mm. Additionally, the thickness of the severely bulging tee joint ranged from 30.7 mm to 43.4 mm. Generally, both the slight bulging part and the bulging tee joint displayed unevenly distributed thicknesses, which might have originated from the extruding process and uneven abnormal bulging. Furthermore, concerning the external diameter results, a similar phenomenon was observed in all the sampled parts. Even the external diameter of the straight pipe reached 223 mm, which could be attributed to slight bulging.

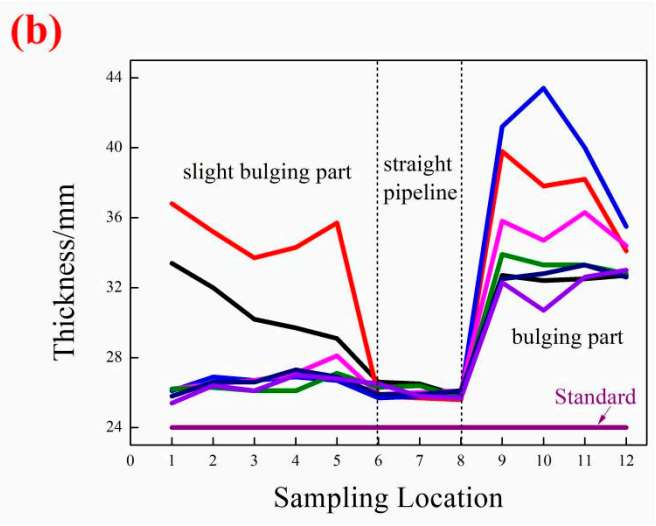

Figure 2. *Cont.*

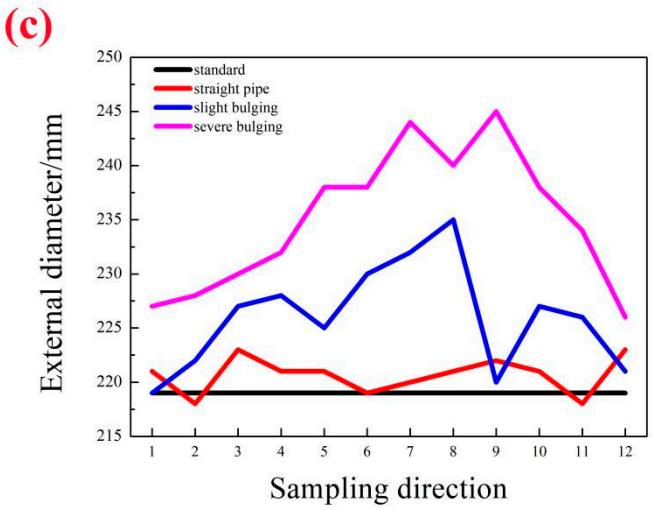

Figure 2. (**a**) Sampling location of the bulging tee joint; (**b**) thickness of the sampling location for the bulging tee joint; (**c**) external diameter of the sampling location for the bulging tee joint.

2.3. Chemical and Mechanical Properties

Full quantitative spectral analysis was conducted to analyze the chemical composition of the abnormal bulging tee joints (Table 1). The results reveal that the chemical composition of the failure samples corresponds to the design standard for P11.

Table 1. Results of the chemical analysis (wt%).

	C	Si	Mn	*p*	S	Cr	Mo
Bulging tee joint	0.132	0.783	0.434	0.0063	0.0094	1.13	0.553
Slight bulging tee joint	0.144	0.805	0.418	0.0128	0.0150	1.11	0.561
Straight pipe	0.0954	0.595	0.358	0.0053	0.0093	1.03	0.486
A335M P11	≤0.15	0.5–1.0	0.3–0.6	≤0.025	≤0.025	1.0–1.5	0.44–0.65

The mechanical properties of the sampled bulging tee joints are presented in Table 2. For the severe bulging part of the samples, the yield strength, tensile strength, elongation after fracture, Brinell hardness, and impact energy are 594.5 MPa, 655.48 MPa, 27.2%, 166.72 HBW, and 136.3 Akv/J, respectively. Additionally, for the slight bulging tee joint, the yield strength, tensile strength, elongation after fracture, and impact energy are 407.12 MPa, 623.85 MPa, 32.3%, and 149.34 HBW, respectively. As for the straight pipe, the yield strength, tensile strength, elongation after fracture, and impact energy are 522.22 MPa, 562.27 MPa, 32%, and 132.45 HBW, respectively.

Table 2. Results of the mechanical properties.

	Yield Strength/MPa	Tensile Strength/MPa	Elongation/%	Impact Energy A_{kv}/J	Hardness/ HBW
Bulging tee joint	594.5	655.48	27.2	136.3	166.72
Slight bulging tee joint	407.12	623.85	32.3	206.3	149.34
Straight pipe	522.22	562.27	32	266.7	132.45
A335M P11	207	415	30	35	≤197

The tensile strength and yield strength of all sampling locations are significantly higher than the standard of ASTM335 P11. The variation in tensile strength for all samples follows the pattern: severe bulging tee joint > slight bulging tee joint > straight pipe.

Regarding elongation after fracture, both the slight bulging tee joint and straight pipe meet the standard of ASTM335 P11, except for the severe bulging tee joint. The variation in elongation after fracture can be summarized as follows: severe bulging tee joint < slight bulging tee joint < straight pipe.

All samples exhibit an impact energy greater than the standard of ASTM335 P11, following this pattern: severe bulging tee joint < slight bulging tee joint < straight pipe. Additionally, all samples have lower Brinell hardness than the standard of ASTM335 P11. The regularity of Brinell hardness for all samples is summarized as follows: severe bulging tee joint > slight bulging tee joint > straight pipe.

Based on the above mechanical properties, it can be concluded that both the two bulging tee joints and the straight pipe demonstrate high strength along with low toughness. Moreover, severe bulging results in higher strength but lower toughness.

2.4. Metallographic Observation for a Bulging High-Pressure Steam Tee Joint

In order to investigate the relations between the mechanical properties and microstructure, the severe bulging part, slight bulging part and straight part of the failure pipes were sampled for a metallographic observation (Figure 3).

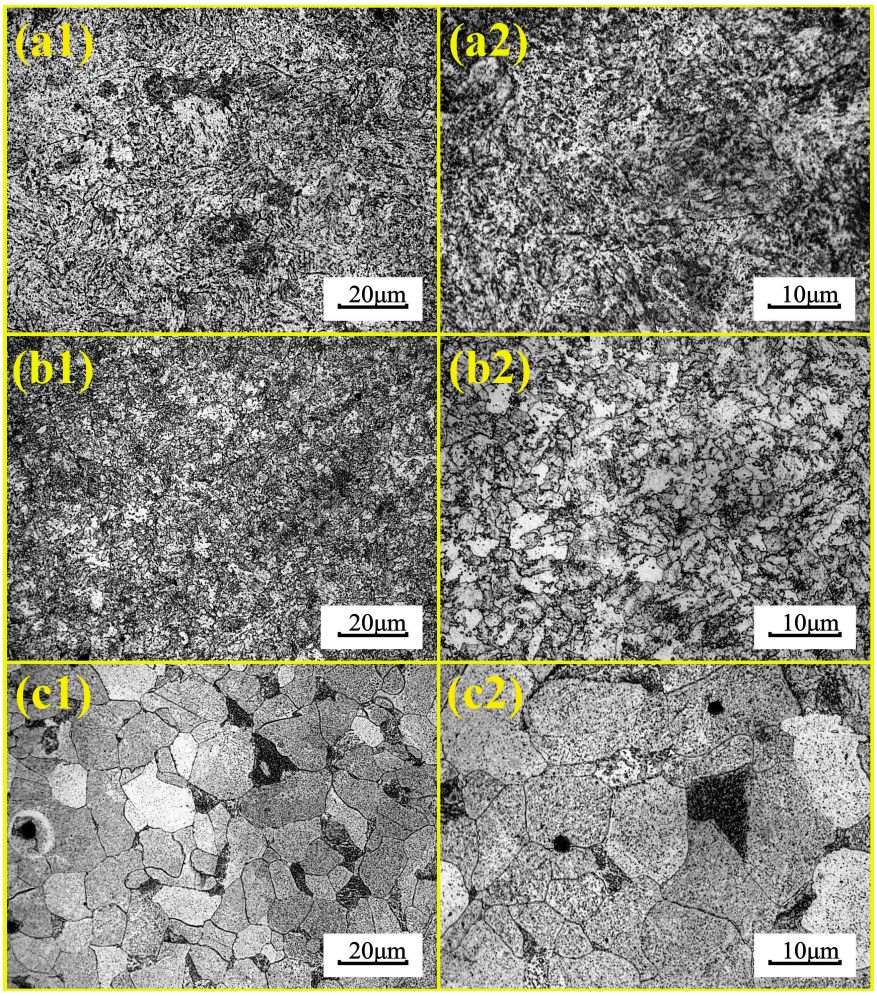

Figure 3. (**a1**,**a2**) Metallographic image of the severe bulging tee joint; (**b1**,**b2**) metallographic image of the slight bulging tee joint; (**c1**,**c2**), metallographic image of the straight pipe.

According to Figure 3(a1,a2), the severe bulging tee joints present the microstructure of pearlite and ferrite without creep cavity and creep crack. However, the relevant structure of pearlite appeared to have severe spheroidization, while the quantity of carbide was

precipitated in the ferritic structure. Additionally, the slight bulging sample (Figure 3(b1,b2)) depicted a similar microstructure of pearlite and ferrite with no creep cavity and creep crack to the severe bulging sample. The relevant structure of pearlite exhibited less severe spheroidization and a medium degree of precipitation for the carbide in the ferrite structure. For the straight pipe in Figure 3(c1,c2), only slight spheroidization in the pearlite structure as well as a mild degree of precipitation for the carbide in the ferrite structure were observed, while no creep cavity and creep crack were found.

Generally, the above observed results reveal that severe abnormal bulging was accompanied by the severe precipitation of carbide in ferrite as well as severe spheroidization in pearlite. No creep cavity and creep crack were found, illustrating that creep has no effect on abnormal bulging.

2.5. Numerical Simulation

2.5.1. Mathematical Model

As the service medium in the bulging tee joints consist of steam vapor and condensed water, a multi-phase flow model was used. This model can simulate a multi-phase flow under different phase velocity conditions, including the continuity, momentum, energy equations and volume fraction equation of the second phase [21].

Continuity equation

$$\frac{\partial}{\partial t}(\rho_m) + \nabla \cdot (\rho_m \vec{\nu}_m) = 0 \tag{1}$$

$\vec{\nu}_m$ represents the average mass velocity, m/s; ρ_m represents the mixed density, kg/m^3; and t is time, s.

Momentum equation:

$$\begin{array}{ll} \frac{\partial}{\partial t}(\rho_m \vec{\nu}_m) & +\nabla \cdot (\rho_m \vec{\nu}_m \vec{\nu}_m) \\ & = -\nabla p + \nabla \cdot [\mu_m (\nabla \vec{\nu}_m + \nabla \vec{\nu}_m^T)] + \rho_m \vec{g} + \vec{F} \\ & +\nabla \cdot (\sum_{i=1}^{n} \alpha_i \rho_i \vec{\nu}_d \vec{\nu}_d) \end{array} \tag{2}$$

$\vec{g}$ represents the acceleration of gravity, m^2/s; $\vec{F}$ represents the volume force, N; μ_m represents the mixed viscosity, Pa•s; p represents the pressure, Pa; n represents the number of phases; α_i represents the volume fraction of the i phase; $\vec{\nu}_d$ represents the slip velocity of the i phase, m/s; and ρ_i represents the density of the i phase, kg/m^3.

Energy equations:

$$\begin{array}{c} \frac{\partial}{\partial t} \sum_{i=1}^{n} (\alpha_i \rho_i E_i) + \nabla \cdot \sum_{i=1}^{n} (\alpha_i \vec{\nu}_i (\rho_i E_i + p)) \\ = \nabla \cdot (K_e \nabla T) + S_E \end{array} \tag{3}$$

$$E_i = h_i - \frac{p}{\rho_i} + \frac{\nu_i^2}{2} \tag{4}$$

where n represents the number of phases; K_e represents the effective heat conductivity, W/(m•K); S_E represents the volume heat source; h_i represents the enthalpy of the i phase; $\vec{\nu}_i$ represents the velocity of the i phase, m/s; and T represents the temperature, K.

Volume fraction equation of the second phase:

$$\frac{\partial}{\partial t}(\alpha_i \rho_i) + \nabla \cdot (\alpha_i \rho_i \vec{\nu}_m) = -\nabla \cdot (\alpha_i \rho_i \vec{\nu}_d) \tag{5}$$

Standard k-ε model:

$$\begin{array}{c} \rho \frac{\partial k}{\partial t} = \frac{\partial}{\partial x_i} \left[\left(\mu + \frac{\mu_t}{\sigma_k} \right) \frac{\partial k}{\partial x_i} \right] + G_k + G_b - \rho \varepsilon - Y_M \\ \rho \frac{\partial \varepsilon}{\partial t} = \frac{\partial}{\partial x_i} \left[\left(\mu + \frac{\mu_t}{\sigma_k} \right) \frac{\partial \varepsilon}{\partial x_i} \right] + C_1 \frac{\varepsilon}{k} (G_k + C_3 G_b) - C_2 \rho \frac{\varepsilon^2}{k} \end{array} \tag{6}$$

k represents the turbulent kinetic energy, m^2/s^2; ε represents the turbulent dissipation rate, m^2/s^3; G_k represents the turbulent kinetic energy term caused by the laminar velocity gradient; G_b represents the turbulent kinetic energy term caused by buoyancy; Y_M represents the effect of compressible turbulent fluctuating expansion on the total dissipation rate; C_1, C_2, C_3 are constants; σ_k and σ_ε are the turbulent Prandtl numbers; u_t represents the turbulent velocity, m/s; μ represents the viscosity, Pa•s; μ_t represents the turbulent viscosity coefficient; and x represents the rectangular coordinate direction.

Computational model

The governing equations are three-dimensional unsteady N-S equations, and the finite volume method is used to calculate the governing equations. The standard simple method is used for pressure velocity coupling, the standard k-ε model is used for the turbulence model, and the VOF model is used for the multi-phase flow model.

Boundary conditions

The conditions of all interfaces in contact with fluid adopt the pipe wall condition, and conditions near the wall adopt the standard wall functions. Since the fluid is a mixture of liquid and gas/vapor, the gravity term must be considered in the simulation.

2.5.2. Simulation of the Precipitation for Condensed Water

In order to clarify the relationship between service conditions and the variation in microstructure and mechanical properties mentioned above, modeling was conducted for the severe bulging tee joint, slight bulging tee joint and straight pipe to simulate the actual service condition, including the fluid inside the pipe, pipe wall and external thermal insulating layer. Steam, 515 °C and 11.6 MPa were selected as the pipe medium, temperature and operating pressure, respectively, while the regulating valve and safety valve maintained the normal shut-down condition. As shown in Figure 4 regarding the distribution of temperature inside the pipe wall, it is observed that temperature inside the main pipe part was 515 °C. As the pressure increases, the regulating valve and safety valve are turned on to vent some high-pressure steam to the mid-pressure steam pipes, thereby increasing the temperature of the remote branch pipes connected to the regulating valve and safety valve. However, during the shut-down condition of the regulating valve and safety valve, the steam becomes stagnant, causing the temperature of the remote branch pipes to decrease significantly below 322.13 °C, which is the saturated steam temperature under the corresponding pressure condition. As a result, the temperature of the remote branch pipes ranges from 515 °C to 29 °C during the cyclic variation of shut-down and turn-on conditions. Therefore, the precipitation of condensed water is likely to occur in the remote branch pipes connected to the regulating valve.

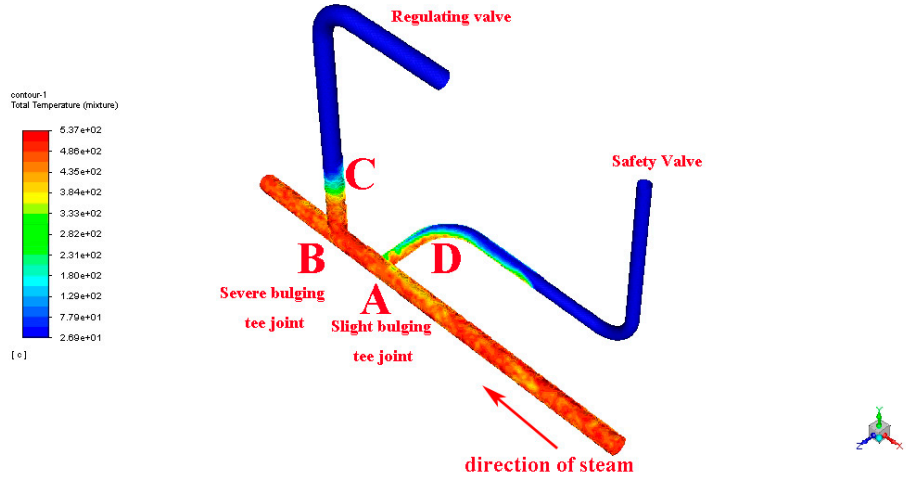

Figure 4. Distribution of temperature inside the bulging tee joint.

According to the distribution of the liquid phase in the inner side of the pipe in Figure 5a,b, the condensed water basically distribute in the inner side of the pipe wall, illustrating that the condensed water would not evenly distribute in the high-pressure steam, but would drop on the tee joint along the vertical pipe. As the surface temperature of the tee joint reaches 515 °C, the process of condensed water dropping would generate a quenching effect to increase the hardness of the tee joint.

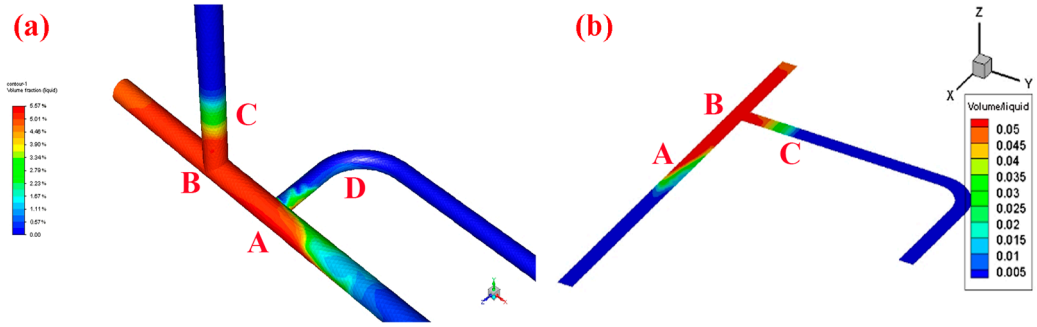

Figure 5. Volume (**a**) and cross-sectional distribution (**b**) of the liquid phase inside the bulging tee joint.

2.5.3. Simulation of Stress Field and Condensed Water Dropping on the Hot Cylinder

In order to further investigate the mechanism of abnormal bulging, numerical modeling was conducted to simulate the subsequent variation in the temperature field and stress field of a hot cylinder induced by a single condensed water droplet, while a spherical-shaped droplet with a diameter of 2 mm and 500 °C surface temperature was selected as the simulated parameter.

As depicted in Figures 6 and 7, the temperature of a condensed water droplet ranges from 500 °C to 200 °C, which is responsible for the generation of alternating thermal stress. It can be seen that a condensed water droplet would be vaporized after dropping on the inner side of pipe wall, subsequently absorbing the heat to generate a rapid decrease in the inner surface temperature of the pipe wall. Therefore, the continuous dropping of a condensed water droplet would produce a rapid cooling effect similar to the quenching process, which would obviously increase the hardness of the tee joint. However, the droplet would finally be vaporized by a high inner surface temperature, increasing the inner surface temperature of the tee joint to a saturated steam temperature. As the constant variation in temperature field and stress generate, regions of high stress would be generated at the inner side of the pipe wall. According to Figure 7a–d, it can be seen that stress produced by a condensed water droplet ranges from 532.8 MPa to 59 MPa by continuously applying it to the tube wall of the tee joint. Combined with the variation in the temperature field in Figure 6, the temperature of the severe bulging tee joint and slight bulging tee joint alternates. Due to the cyclic transformation and dropping of condensed water, the alternating thermal stress and ratcheting effect would be generated, causing abnormal bulging in the tee joints [22–26]. The dynamic variation in the temperature field and phase field induced by the transformation of condensed water is attached in the Supplementary Files.

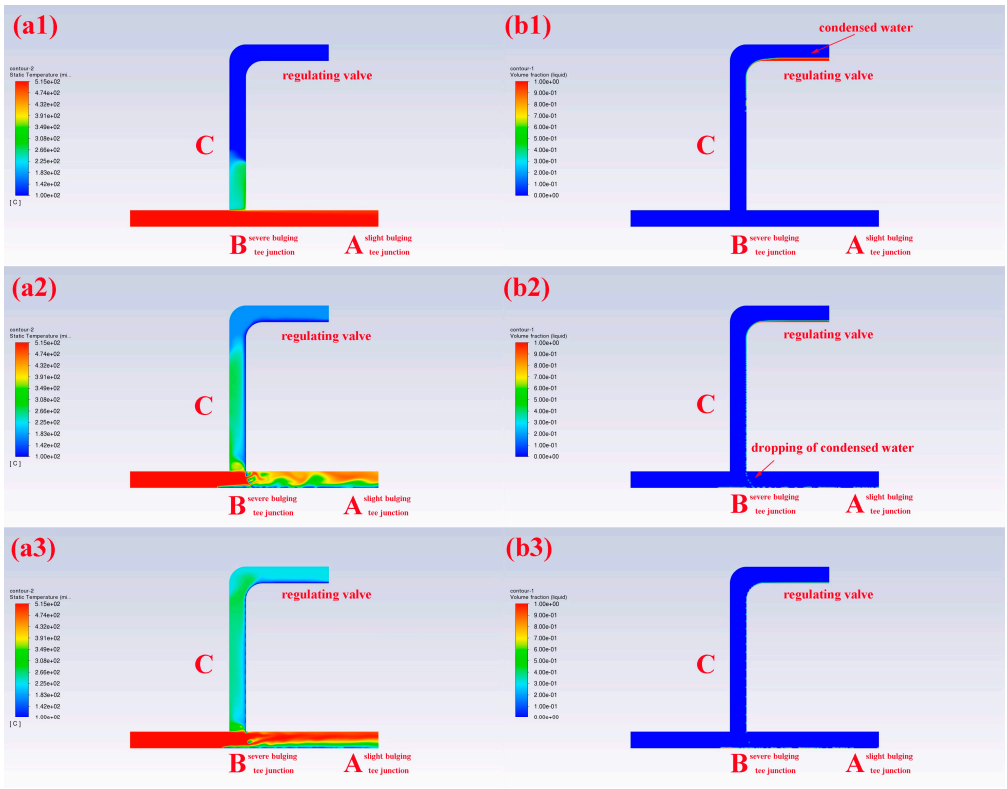

Figure 6. Variation in (**a1**–**a3**) the temperature field and (**b1**–**b3**) phase field induced by the transformation of condensed water.

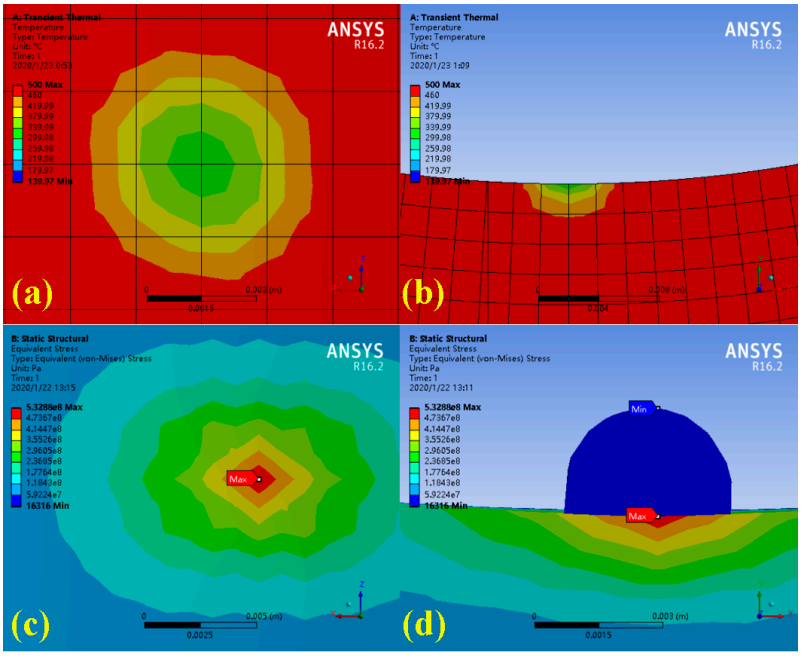

Figure 7. (**a**,**b**) Temperature field and (**c**,**d**) stress field of condensed water droplets on the bulging tee joint.

3. Discussion

Generally, in accordance with the external dimension and thickness results, bulging was observed on both of the tee joints, while slight bulging occurred on the straight pipe. The chemical composition results reveal that the composition of the bulging pipe

corresponded to the design standard of the P11 alloy steel. Furthermore, it could be concluded that both the bulging tee joint as well as the straight pipe possess features of high strength and low toughness on the basis of room-temperature mechanical properties and hardness. For the metallographic results, all the sampling parts depict a microstructure of pearlite combined with ferrite, while severe bulging leads to severe spheroidization in pearlite along with the severe precipitation of carbide inside the ferrite. No creep cavity and creep crack were observed. Therefore, the dominant mechanism of bulging could be attributed to thermal fatigue, while pearlite spheroidization is the secondary mechanism. The severe bulging tee joint is in front of the medium-pressure regulating valve, which belongs to the main steam pipe for regulating the super-high pressure steam pipe of the pyrolyzer. The regulating valve is shut down under normal conditions, while the temperature reduces along with the blocking of steam. As the regulating valve shuts down, the temperature of the pipe in front of the regulating valve keeps decreasing until it is lower than the saturated steam temperature, then generating condensed water. The precipitation of condensed water drops down to the tee joints along the standpipes, decreasing the temperature of the tee joint. However, as the condensed water droplet closes to the main steam pipe, condensed water is vaporized alongside the increase in temperature until reaching the main steam temperature. This circulation generates alternating thermal stress, which is continuously applied on the failed tee joints. Occurrences of ratcheting and quenching are attributed to the alternating thermal stress and cyclic dropping of condensed water, which increases the hardness and strength of tee joints along with a deterioration in toughness. Meanwhile, the application of high temperature and thermal stress further accelerates the pearlite spheroidization. Furthermore, the precipitation of condensed water is not evenly distributed in high-pressure steam, causing the concentration of the liquid phase inside the tube wall. Consequently, condensed water drops to the surface of tee joints with a high temperature and generates a phenomenon like quench, which is attributed to the increasing of hardness as well as the deterioration of toughness. A similar phenomenon could be found in mild bulging tee joints and the straight pipe between the two failed tee joints mentioned above.

4. Conclusions and Countermeasures

Based on the physical and chemical inspections, as well as numerical simulations, the following conclusions are summarized:

The pearlites are severely spheroidized, accompanied by the precipitation of carbides in ferrites. No creep voids or cracks are found in the metallographic structure. The bulging deformation of the tee junction accelerates the precipitation of carbides inside the grains, resulting in increased strength and hardness, along with decreased ductility and plasticity. Additionally, the interaction of deformation and cyclic alternating thermal stress accelerates pearlite spheroidization.

The abnormal bulging of the tee junction is attributed to the thermal ratcheting effect induced by the cyclic precipitation of condensed water, with pearlite spheroidization serving as a secondary mechanism.

Countermeasures for improvement are summarized as follows:

(1) Replace the unqualified pipes and conduct inspections on pipes under similar service conditions.
(2) Place emphasis on the inspection and life cycle assessment of high-pressure steam pipes.

Supplementary Materials: The following supporting information can be downloaded at: https://www.mdpi.com/article/10.3390/pr11082288/s1, Video S1: variation of phase field; Video S2: variation of temperature field.

Author Contributions: Conceptualization, Z.S., Z.D., W.L. and Y.L.; methodology, Y.L.; software, Z.S.; validation, W.L. and Y.L.; formal analysis, Z.D. and W.L.; investigation, W.L.; resources, W.L.; data curation, W.L.; writing—original draft preparation, W.L. and Z.S.; writing—review and editing, W.L., Z.S. and Y.L.; visualization, W.L.; supervision, Z.S. and Z.D.; project administration, Y.L.; funding acquisition, W.L. All authors have read and agreed to the published version of the manuscript.

Funding: Financial support by the Projects of Talents Recruitment of Guangdong University of Petrochemical Technology (No. 2022RCYJ2005) and the Open Foundation of Guangdong Provincial key laboratory of Petrochemical Equipment Fault Diagnosis (No. 91720212) are gratefully acknowledged.

Data Availability Statement: Not applicable.

Conflicts of Interest: The authors declare no conflict of interest.

References

1. Vetriselvan, R.; Sathiya, P.; Ravichandran, G. Experimental and numerical investigation on thermal fatigue behaviour of 9Cr 1Mo steel tubes. *Eng. Fail. Anal.* **2018**, *84*, 139–150. [CrossRef]
2. Shami, A.; Moussavi Torshizi, S.E.; Jahangiri, A. Failure Analysis and Remedial Solution Suggestion for Superheater Tubes of a Power Plant Boiler. *Trans. Indian Inst. Met.* **2020**, *73*, 1729–1741. [CrossRef]
3. Huda, Z. Failure Analysis of Steel Superheater Tube Fractured in a Boiler of a Power Plant. *Key Eng. Mater.* **2011**, *462–463*, 467–471. [CrossRef]
4. Maharaj, C.; Dear, J.P.; Morris, A. A Review of Methods to Estimate Creep Damage in Low-Alloy Steel Power Station Steam Pipes. *Strain* **2009**, *45*, 316–331. [CrossRef]
5. Niu, X.; Gong, J.; Jiang, Y.; Bao, J. Creep damage prediction of the steam pipelines with high temperature and high pressure. *Int. J. Pres. Ves. Pip.* **2009**, *86*, 593–598. [CrossRef]
6. Chu, Q.; Zhang, M.; Li, J.; Chen, Y.; Luo, H.; Wang, Q. Failure analysis of a steam pipe weld used in power generation plant. *Eng. Fail. Anal.* **2014**, *44*, 363–370. [CrossRef]
7. Sierra-Espinosa, F.Z.; García, J.C. Vibration failure in admission pipe of a steam turbine due to flow instability. *Eng. Fail. Anal.* **2013**, *27*, 30–40. [CrossRef]
8. Zhang, J.X.; Bai, Y.Q.; Kang, J.; Wu, X. Failure analysis and erosion prediction of tee junction in fracturing operation. *J. Loss Prev. Proc.* **2017**, *46*, 94–107. [CrossRef]
9. Zhang, S. Failure analysis on tee pipe of duplex stainless in an oilfield. *Eng. Fail. Anal.* **2020**, *115*, 104676. [CrossRef]
10. Fang, Y.; Xu, S.; Zeng, Q.; Wang, C.; Song, M. Failure Analysis of Tees on Heat Exchanger Inlet. *J. Fail. Anal. Prev.* **2019**, *19*, 782–791. [CrossRef]
11. Watson, J.F.; Rance, J.M.; Anderson, H.J. Analysis of the fatigue failure of tee pieces forming part of a header in a descaling system in a hot strip rolling mill. *Int. J. Press. Vessel. Pip.* **1996**, *68*, 121–126. [CrossRef]
12. Ashrafizadeh, H.; Karimi, M.; Ashrafizadeh, F. Failure analysis of a high pressure natural gas pipe under split tee by computer simulations and metallurgical assessment. *Eng. Fail. Anal.* **2013**, *32*, 188–201. [CrossRef]
13. Zheng, X.F.; Feng, Y.T.; Niu, X.G.; Wang, Q.; Hao, X.J.; Li, W.B.; Xu, X.X.; Sun, P. Failure Analysis on Tee Joint Crack of Subcritical Power Station Boiler Final Superheater Header. *Adv. Mater. Res.* **2011**, *311–313*, 615–618. [CrossRef]
14. Cao, J.; Ma, W.; Pang, G.; Wang, K.; Ren, J.; Nie, H.; Dang, W.; Yao, T. Failure analysis on girth weld cracking of underground tee pipe. *Int. J. Pres. Ves. Pip.* **2021**, *191*, 104371. [CrossRef]
15. Kumar, S.; Tadge, P.; Mondal, A.; Hussain, N.; Ray, S.; Saha, A. Boiler tube failures in thermal power plant: Two case studies. *Mater. Today Proc.* **2022**, *66*, 3847–3852. [CrossRef]
16. Lyu, Y.; Lian, W.; Sun, Z.; Li, W.; Duan, Z.; Chen, R.; Yu, W.; Shao, S. Failure Analysis of Abnormal Bulging and Cracking for High-Pressure Steam Pipe. *J. Mater. Eng. Perform.* **2022**, *31*, 7277–7289. [CrossRef]
17. Zhang, Y.; Yun, F.; Fang, W.; Wang, H. Analysis on the cause of crack in connection pipeline of subcritical boiler reheater. *IOP Conf. Ser. Earth Environ. Sci.* **2020**, *508*, 12202. [CrossRef]
18. Munda, P.; Husain, M.M.; Rajinikanth, V.; Metya, A.K. Evolution of Microstructure During Short-term Overheating Failure of a Boiler Water Wall Tube Made of Carbon Steel. *J. Fail. Anal. Prev.* **2018**, *18*, 199–211. [CrossRef]
19. Porcaro, R.R.; Faria, G.L.; Godefroid, L.B.; Apolonio, G.R.; Cândido, L.C.; Pinto, E.S. Microstructure and mechanical properties of a flash butt welded pearlitic rail. *J. Mater. Process Tech.* **2019**, *270*, 20–27. [CrossRef]
20. Khalifa, W.; El-Hadad, S. Metallurgical investigation of early failure of heater pipes in a gas complex. *Sci. Rep.* **2023**, *13*, 5300. [CrossRef]
21. Liu, W.; Lyu, Y.; Duan, Z.; Li, W.; Yu, W. Investigation of corrosion sequence in the overhead pipeline of H2S stripper column through CFD models. *Eng. Fail. Anal.* **2022**, *136*, 106187. [CrossRef]
22. Lin, Y.C.; Chen, X.; Chen, G. Uniaxial ratcheting and low-cycle fatigue failure behaviors of AZ91D magnesium alloy under cyclic tension deformation. *J. Alloys Compd.* **2011**, *509*, 6838–6843. [CrossRef]
23. Lin, Y.C.; Liu, Z.; Chen, X.; Chen, J. Uniaxial ratcheting and fatigue failure behaviors of hot-rolled AZ31B magnesium alloy under asymmetrical cyclic stress-controlled loadings. *Mater. Sci. Eng. A* **2013**, *573*, 234–244. [CrossRef]

24. Yang, X. Low cycle fatigue and cyclic stress ratcheting failure behavior of carbon steel 45 under uniaxial cyclic loading. *Int. J. Fatigue* **2005**, *27*, 1124–1132. [CrossRef]
25. Dong, Q.; Yang, P.; Xu, G. Low cycle fatigue and ratcheting failure behavior of AH32 steel under uniaxial cyclic loading. *Int. J. Nav. Arch. Ocean* **2019**, *11*, 671–678. [CrossRef]
26. Wang, S.; Yan, X.; Lu, F.; Lei, S.; Chen, R. Modelling of Ratchet Growth in TATB-Based Charge under Thermal Cycling. *Propellants Explos. Pyrotech.* **2022**, *47*, e202100271. [CrossRef]